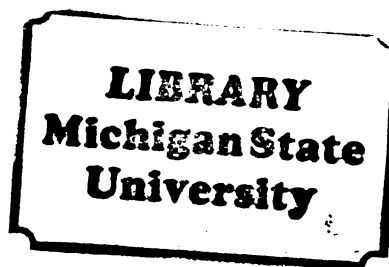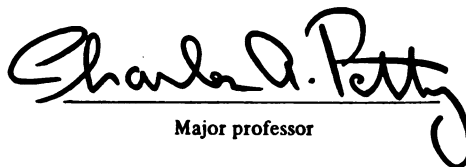This is to certify that the

thesis entitled

AN APPROXIMATE PRESSURE DISTRIBUTION FOR A
VISCOELASTIC FLUID IN CONICAL FLOW

presented by

Khuong Van Nguyen

has been accepted towards fulfillment
of the requirements for

Master of Science _____ degree in Chemical Engineering

_____
Major professor

Date November 1, 1982

AN APPROXIMATE PRESSURE DISTRIBUTION FOR A
VISCOELASTIC FLUID IN CONICAL FLOW

By

Khuong Van Nguyen

A THESIS

Submitted to
Michigan State University
in partial fulfillment of the requirements
for the degree of

MASTER OF SCIENCE

Department of Chemical Engineering

1982

ABSTRACT

AN APPROXIMATE PRESSURE DISTRIBUTION FOR A
VISCOELASTIC FLUID IN CONICAL FLOW

By

Khuong Van Nguyen

A theory for estimating the isotropic pressure distribution for viscoelastic fluids in converging flow is developed. The theory assumes that to first order the kinematic structure of a pure radial converging flow is unaffected by the presence of a high molecular weight polymer. The normal stresses and shear stresses are estimated by using a retardation model for viscoelastic fluid. The isotropic pressure distribution is determined by integrating the radial component of the force balance. The results show that under certain conditions a positive minimum in the isotropic pressure occurs near the contraction and, thereby, provides a quantitative explanation of 'hazing.' Furthermore, a simple criterion for flow instability is suggested which relates the applied pressure $\hat{P}_\infty$, the fluid viscosity μ, and the fluid retardation time λ. Instability occurs when $\lambda \hat{P}_\infty / \mu \leq 0.015$.

This thesis is dedicated to my parents and my wife, Linh Nguyen, whose love and concern have meant much to me.

ACKNOWLEDGMENTS

TABLE OF CONTENTS

LIST OF FIGURES

NOTATION

CHAPTER 1

INTRODUCTION

The Physical Problem

Converging flows of viscoelastic materials are encountered
in numerous processes involving polymer melts and solutions. These
flows have probably been studied as much for their unique and unusual
behavior as for their pragmatic importance. For instance, an aqueous
solution of polyacrylamide undergoing a 4:1 contraction at low
Reynolds numbers can not only support a symmetric vortex flow off
the axis of symmetry but also a flow 'bulge' simultaneously on the
axis (see Figure 1.1a). Cable and Boger [1978a,b] recently presented
the results of a comprehensive experimental study of these structures
and their stability. Just as curious is the phenomenon illustrated
by Figure 1.1b, which shows a fairly large bubble retarded at the
mouth of a contraction by an accelerating viscoelastic fluid. Metzner
[1967] attributed this phenomenon to the large normal stresses which
usually accompany a converging viscoelastic fluid. These normal
stresses may also cause a minimum in the isotropic pressure just
before a contraction and, thereby, explain the phenomenon known
as 'hazing' illustrated in Figure 1.1c (Metzner et al., 1969). Fur-
thermore, elastic forces also have important consequences in polymer
extrusion as shown in Figure 1.1d and discussed by Denn [1980].

"Bulge"

$R_e = 100$

4:1 Contraction

a.

(Cable & Boger, 1978)

"Bubble"

b.

(Uebler, 1966)

"Haze"

Clear

Clear

Clear

c.

(Metz ner, et al., 1969)

Low Rate

High Rate

Melt Fracture
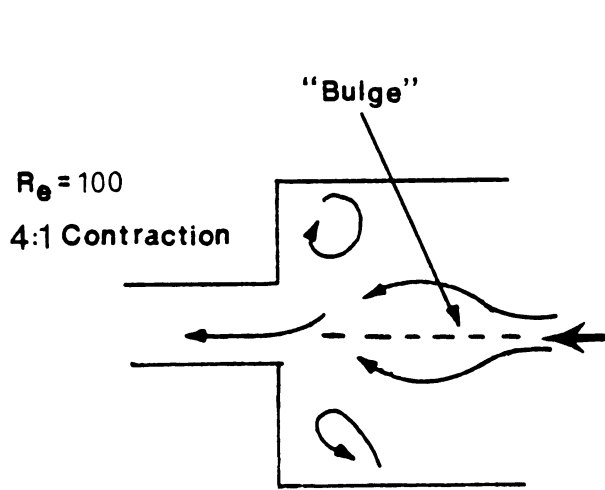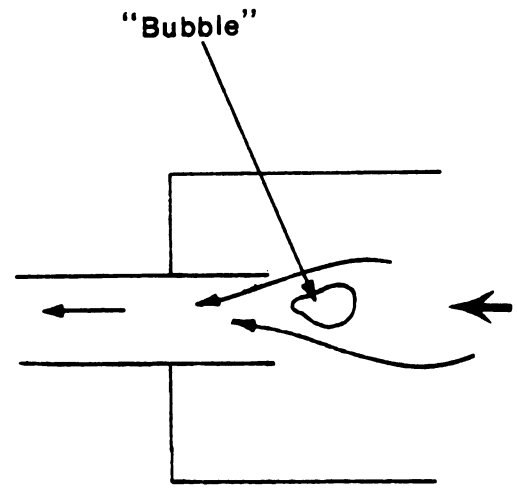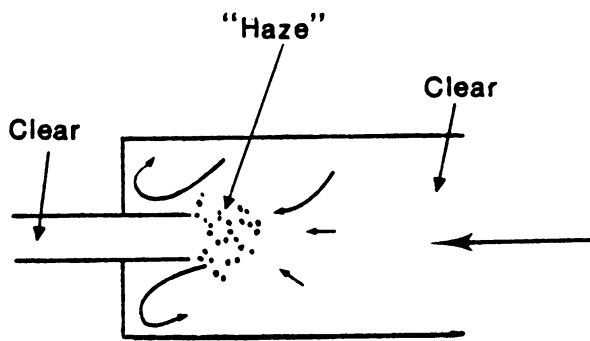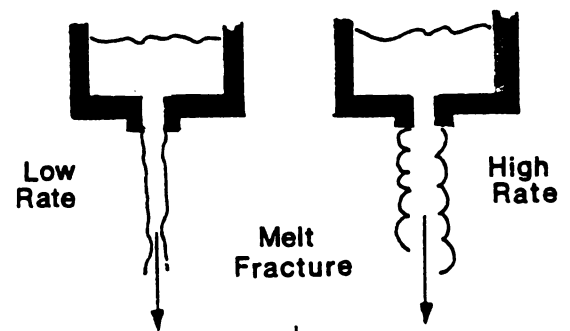
d.

(Denn, 1980)

Figure 1.1.   Schematic of Flow Phenomenon

Numerous experimental and theoretical studies of converging

flows have appeared in the literature for both Newtonian and visco-

elastic fluids. An early experimental study by Bond [1925] on flow

through wide angle cones for Newtonian fluids at low Reynolds numbers

confirmed some of the qualitative features of the creeping flow

solution reported by Harrison [1919]. A very interesting analysis

of viscous incompressible flow inside a cone was reported by

Ackerberg [1965]. Ackerberg correctly pointed out the failure of

the Stokes solution in the apex region and developed a solution

strategy based on an inner and outer expansion using a boundary

layer flow and a 'new' core flow. The resulting calculation gave

the interesting result of a vortex motion near the apex and on the

line of symmetry similar to the structure observed by Cable and

Boger [1978a] for a viscoelastic fluid. Of course, Ackerberg's theo-

retical result occurs because of the interplay between inertial

and viscous forces whereas the 'bulge' observed by Cable and Boger

is probably due to elastic effects, although a weak Reynolds number

dependence also seems likely.

Shümmer [1967] studied the flow of a viscoelastic fluid in

a converging two dimensional channel using a third order viscoelastic

model. A sketch of the flow pattern predicted by his perturbation

analysis is shown in Figure 1.2 along with the result reported by

Ackerberg [1965]. Black and Denn [1976] also used a perturbation

analysis to study two dimensional converging flows of a Maxwell

model. The analysis predicted a backflow along the center line for

(a) Newtonian Fluid

(b) 3rd Order Fluid
$(R_e < < < 1)$
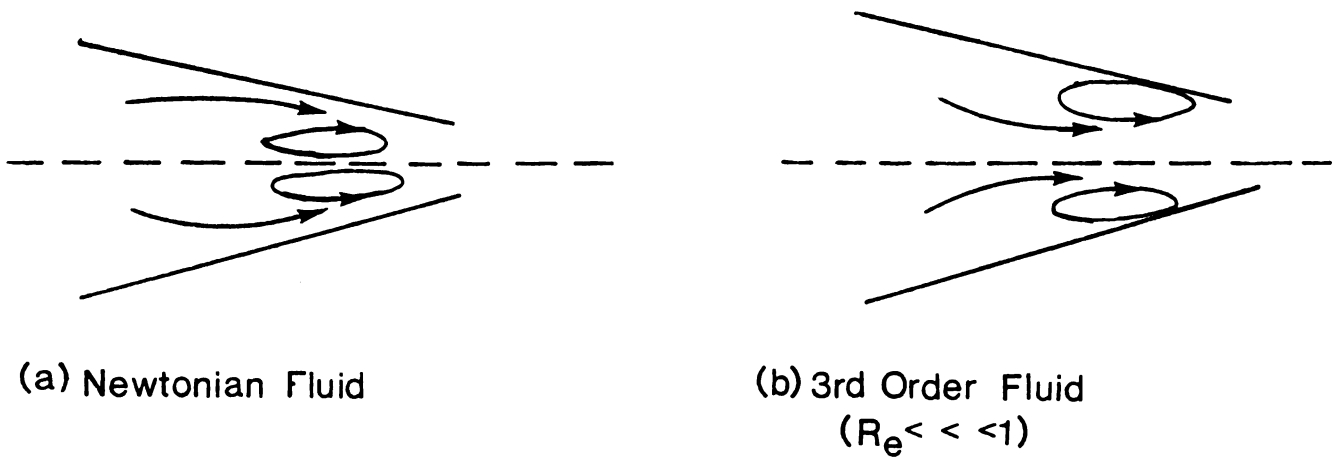
Figure 1.2.   Schematic of Flow Pattern Predicted Theoretically

a Weissenberg number less than 0.4. Strauss [1975] has observed
this type of phenomenon for viscoelastic fluids between two con-
verging planes.

Black and Denn also concluded that 'sink' flow (see Chapter 2)
was probably a good basis for a perturbation analysis for conical
geometries with apex angles less than 90°. Oka and Takami [1967]
successfully used the 'sink' flow model to study the conical flow
of a power law fluid as Kaloni [1965b] did earlier for an Oldroyd
model.

Kaloni [1965a] also used an Oldroyd model to study converging
flows in a two dimensional channel. He showed that in the first
order approximation the kinematic structure of the flow is unaffected
and remains the same as in the case for ordinary viscous fluids (i.e.,
two dimensional 'sink' flow). However, the distribution of forces
are affected. Tanner [1966] has also proved this for a second-
order fluid. These observations of Kaloni and Tanner are significant
inasmuch as they provide a key idea which underlies this study (see
Chapter 2). We emphasize, however, that the problem examined here
is three dimensional and there is no guarantee that the kinematic
structure of weak viscoelastic flows in conical geometries is
unaffected in a first approximation.

The practical importance of entrance flows in engineering
has been discussed lucidly by Duda and Vrentas [1973]. The magni-
tude of the excess pressure drop caused by accelerating flows and
the physical size of the separation zone (see Figure 1.1) are

significant for viscoelastic fluids. Thus, fluid transport from
an upstream reservoir to a smaller tube proceeds through a relatively
slender conical region. The important factors which control this flow
for polymer solutions remain unclear but certainly any theoretical
analysis must consider one of the many constitutive models contain-
ing viscous and elastic effects.

Perera and Walters [1977] have studied the effect of high
elasticity involving viscoelastic fluids and abrupt changes in
geometry using a model of the Maxwell-Oldroyd type. A similar
model was employed by Leslie [1960] to study slow flow of a
viscoelastic liquid past a rigid sphere and by Wagner and Slattery
[1971] for droplets. In Chapter 2, a special case of this model,
namely,

$$\hat{\underset{\approx}{\tau}} = 2\mu \left[\hat{\underset{\approx}{S}} + \lambda \frac{S \hat{\underset{\approx}{S}}}{S t} \right] \tag{1.1}$$

will be used to estimate the distribution of forces in conical flow.
In Equation (1.1) μ is a shear viscosity and λ is a retardation
time. Although both of these material parameters should be con-
sidered as scalar functions of the kinematic invariants of the strain
rate $\underset{\approx}{S}$, we follow the lead of many others (see, especially, the
discussion in Black and Denn, 1975) and consider these as constants.

Equation (1.1) contains the physical idea that the kinematic
structure of the flow, as described by the strain rate $\underset{\approx}{S}$, does not

respond instantaneously to sudden change in the stress $\underset{=}{\tau}$. Unlike

a Newtonian fluid, the flow is retarded by intrinsic elastic forces

and thus a fluid element requires some finite amount of time to

adjust to new surroundings. The temporal operator, which appears

in Equation (1.1), is the familiar Oldroyd time derivative defined

by

$$\frac{\delta \underset{\sim}{S}}{\delta t} \equiv \frac{\partial \underset{\sim}{S}}{\partial t} + \underset{\sim}{u} \cdot \nabla \underset{\sim}{S} + (\nabla \underset{\sim}{u})^{T} \cdot \underset{\sim}{S} + \underset{\sim}{S} \cdot \nabla \underset{\sim}{u} \ . \qquad (1.2)$$

Even if the flow is steady in an Eulerian frame of reference, the

remaining terms in Equation (1.2) still make important contributions

for converging flows which are really unsteady in a Lagrangian

sense.

Objectives

The purpose of this study is to develop some understanding

of converging flows of viscoelastic fluids governed by Equation (1.1).

Although the approach is elementary, it should nevertheless provide

a basis for a more quantitative study. Our specific goal will be

to estimate the distribution of forces (isotropic pressure, normal

stresses, and shear stresses) induced by radial flow from a large

reservoir to a small contraction.

Because the underlying flow model includes an inward radial

flow to a point (sink), the velocity and pressure necessarily become

unbounded at the contraction. This is not a major concern for estimating the effects of elasticity far from this singularity but, unfortunately, most of the interesting results illustrated in Figure 1.1 occur near the contraction. Comparing the behavior of two models near their singular points may still provide some useful insights regarding the location and relative sizes of the flow domains which develop unusually large stresses. For example, radial flow of a Newtonian fluid toward a point sink generates a zero pressure distribution on a surface surrounding the contraction. The pressure is negative within this domain (see Figure 2.7). Obviously, this is unphysical and the fluid easily prefers a secondary motion rather than one which induces unbounded stresses. By comparing the pathological features of 'sink' flow for Newtonian and viscoelastic fluids some deductions regarding the onset of secondary motions may be inferred. The attractiveness of this suggestion lies in the simplicity of the analysis which follows.

CHAPTER 2

THEORY

Fundamental Equations

Figure 2.1 shows the geometry of the flow. Spherical coordinates are used with $\hat{r} = 0$ located at the contraction; the parameter d represents the diameter of the small capillary. The flow is entirely radial and axisymmetric, so the velocity vector can be written as

$$\hat{\underline{u}} = \hat{u}_r(\hat{r}, \theta)\, \underline{e}_r \quad , \tag{2.1}$$

where $\hat{u}_r$ is the radial component.

The continuity equation (see page 83 of Bird et al., 1960) requires

$$\hat{r}^2 \hat{u}_r = \text{constant} \quad , \tag{2.2}$$

which shows that $\hat{u}_r$ is unbounded for $\hat{r} \to 0$ if we insist on (2.1) thoughout the flow domain.

Figure 2.1. Definition of Geometric Parameters

The bulk average velocity

$$U_b \cong 4Q/\pi \, d^2 \quad , \tag{2.3}$$

and the diameter of the small capillary d are used as characteristic velocity and length scales. The stresses are made dimensionless by using the volumetric flow rate Q, the viscosity coefficient μ, and the diameter d. Thus, a dimensionless applied pressure at $r = \infty$ is defined as

$$P_\infty \cong \frac{\pi \, d^3 \, \hat{P}_\infty}{\mu \, Q} \tag{2.4}$$

It will be useful to remember that increases in Q correspond to decreases in P_∞ for fixed $\hat{P}_\infty$.

The governing dimensionless equation of motion for steady state creeping flow is

$$\nabla \cdot \underline{\underline{T}} = 0 \tag{2.5}$$

where

$$\underline{\underline{T}} = -p\underline{\underline{I}} + \underline{\underline{\tau}} \quad . \tag{2.6}$$

The constitutive model proposed for $\underset{\sim}{\tau}$ is given by Equation (1.1). In dimensionless form this becomes

$$\underset{\sim}{\tau} = 2\left(\underset{\sim}{S} + W\frac{\delta\underset{\sim}{S}}{\delta t}\right) \qquad (2.7)$$

where the Weissenberg number, defined by

$$W \equiv \frac{\lambda u_b}{d} \quad , \qquad (2.8)$$

compares an intrinsic time for retardation with a characteristic time for the flow, i.e., $\frac{d}{u_b}$. This parameter and P_∞ determine the distribution of forces in the infinite reservoir.

Boundary conditions for the problem studied include no slip at the wall,

$$\hat{u}_r(\hat{r}, \pi/2) = 0 \quad ; \qquad (2.9)$$

symmetry about the axis,

$$\left.\frac{\partial u_r}{\partial \theta}\right|_{\theta=0} = 0 \qquad ; \qquad (2.10)$$

and,

$$\hat{p} = \hat{P}_\infty \quad , \quad \hat{r} = \infty \quad . \qquad (2.11)$$

Component Equations

For axisymmetric flows in spherical coordinates the two relevant component equations (made dimensionless) associated with Equation (2.5) are

$$\frac{\partial p}{\partial r} = \frac{1}{r^2} \frac{\partial}{\partial r} \left(r^2 \, \tau_{rr} \right)$$

$$+ \frac{1}{r \sin\theta} \frac{\partial}{\partial \theta} \left(\tau_{r\theta} \, \sin\theta \right)$$

$$- \frac{\left(\tau_{\theta\theta} + \tau_{\phi\phi} \right)}{r} \tag{2.12}$$

$$\frac{\partial p}{\partial \theta} = \frac{1}{r^2} \frac{\partial}{\partial r} \left(r^2 \, \tau_{r\theta} \right)$$

$$+ \frac{1}{r \sin\theta} \frac{\partial}{\partial \theta} \left(\tau_{\theta\theta} \, \sin\theta \right) \tag{2.13}$$

$$+ \frac{\tau_{r\theta}}{r} - \frac{\cot\theta}{r} \, \tau_{\phi\phi}$$

The nine component equations for (2.7) in spherical coordinates are tedius, but not difficult to derive. For axisymmetric radial flow, the result is (see Bhatnagar and Rajagopalan, 1967)

$$\tau_{rr} = 2 \frac{\partial u_r}{\partial r} + 2 W \left\{ u_r \frac{\partial^2 u_r}{\partial r^2} + 2 \left(\frac{\partial u_r}{\partial r} \right)^2 \right\} \tag{2.14}$$

$$\tau_{\theta\theta} = 2\frac{u_r}{r} + 2W \left\{ \frac{u_r}{r}\frac{\partial u_r}{\partial r} + \frac{1}{r^2}\left(\frac{\partial u_r}{\partial\theta}\right)^2 \right. \tag{2.15}$$

$$\left. + \frac{1}{r^3}u_r^2 \right\}$$

$$\tau_{\phi\phi} = 2\frac{u_r}{r} + 2W \left\{ \frac{1}{r}u_r\frac{\partial u_r}{\partial r} \right. \tag{2.16}$$

$$\left. + \frac{1}{r^2\sin\theta}u_r \right\}$$

$$\tau_{r\theta} = \tau_{\theta r} = \frac{1}{r}\frac{\partial u_r}{\partial\theta} + W \left\{ \frac{u_r}{r}\frac{\partial^2 u_r}{\partial r\partial\theta} \right\} \tag{2.17}$$

$$\tau_{r\phi} = \tau_{\phi r} = \tau_{\theta\phi} = \tau_{\phi\theta} = 0 \quad . \tag{2.18}$$

Radial Flow of a Newtonian Fluid

Setting $W = 0$ in Equations (2.14)-(2.17) gives the components of the stress for Newtonian fluid. Inserting the results into Equations (2.12) and (2.13) gives two equations for the unknown functions $p(r,\theta)$ and $u_r(r,\theta)$. Actually, continuity has already imposed itself on the radial dependence of $u_r(r,\theta)$, so an ordinary differential equation for the stream function $\psi(\theta)$, defined by

$$u_r = -\frac{1}{r^2 \sin\theta} \frac{d\Psi}{d\theta} \quad , \tag{2.19}$$

results from the requirement that

$$\frac{\partial^2 p}{\partial\theta\, \partial r} = \frac{\partial^2 p}{\partial r\, \partial\theta} \tag{2.20}$$

The stream function is easily found to be

$$\hat{\Psi}(\theta) = \hat{\Psi}(0)\, \cos^2\theta \quad , \tag{2.21}$$

where

$$\hat{\Psi}(0) = -\frac{Q}{2\pi} \tag{2.22}$$

and Q is the volumetric flow rate. Figure 2.2 shows how the stream function changes with θ for $0 \le \theta \le \frac{\pi}{2}$.

The dimensionless velocity $(\hat{u}_r/u_b)$ can be determined by inserting (2.21) into (2.19) with the result that

$$u_r = -\frac{3}{8} \frac{\cos^2\theta}{r^2} \quad . \tag{2.23}$$

Note that the no slip condition is satisfied at the surface $\theta = \frac{\pi}{2}$. Also, $u_r \to 0$ as $r \to \infty$ and, unfortunately, $u_r \to \infty$ as $r \to 0$. This
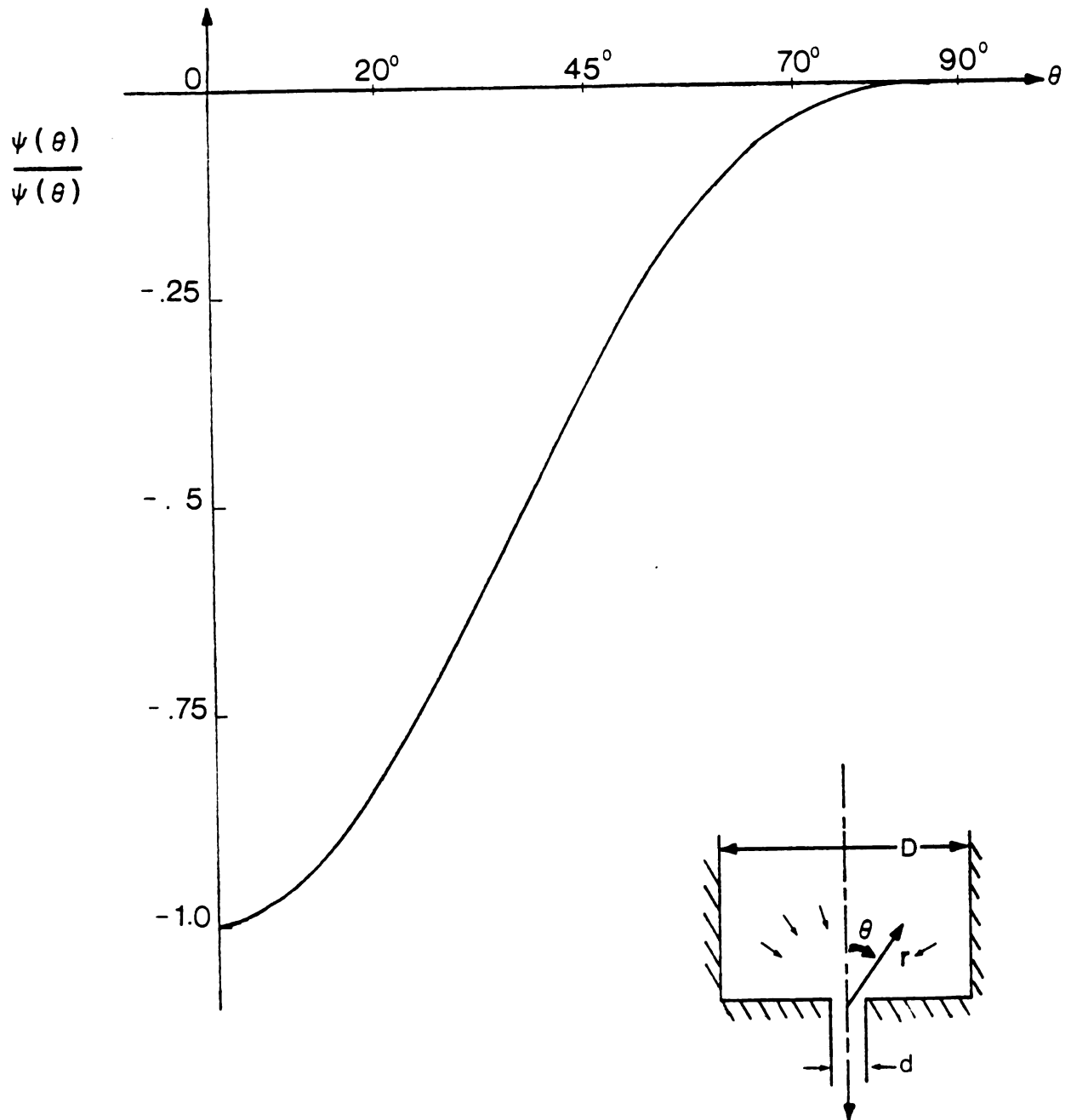
Figure 2.2   Stream Function for Axisymmetric Conical Flow of a
Newtonian Fluid for d/D → 0

velocity field has been used previously by several authors (see Introduction) as a zero order approximation for converging flows of polymer solutions. This is the analog for conical flow of Stokes' classical result for creeping flow past a sphere. Figure 2.3 shows the behavior of u_r with θ for several spherical surfaces. Note that the flow has decayed significantly within a few capillary diameters from the contraction.

Figure 2.4 shows the distribution of shear stresses made dimensionless with $\frac{\mu Q}{\pi d^3}$ and given by

$$\tau_{r\theta} = -3 \frac{\cos\theta \sin\theta}{r^3} \qquad (2.24)$$

$\tau_{r\theta} \cong 1$ corresponds to a pressure drop needed for a flow rate Q through a capillary tube having an L/d of only 1/128! Thus the magnitude of the shear stress is extremely small even within one diameter of the singular point. On the other hand, the normal stresses are much larger in magnitude. However, the shear stresses still play a key role for the Newtonian case since the normal stress terms in Equation (2.12) balance each other identically. One curiosity about Newtonian sink flows follows from Equation (2.24) which shows that the stress is zero at the rigid interface. Thus, the velocity and the shear stress are both zero on the same surface, a feature not normally associated with real viscous flows.

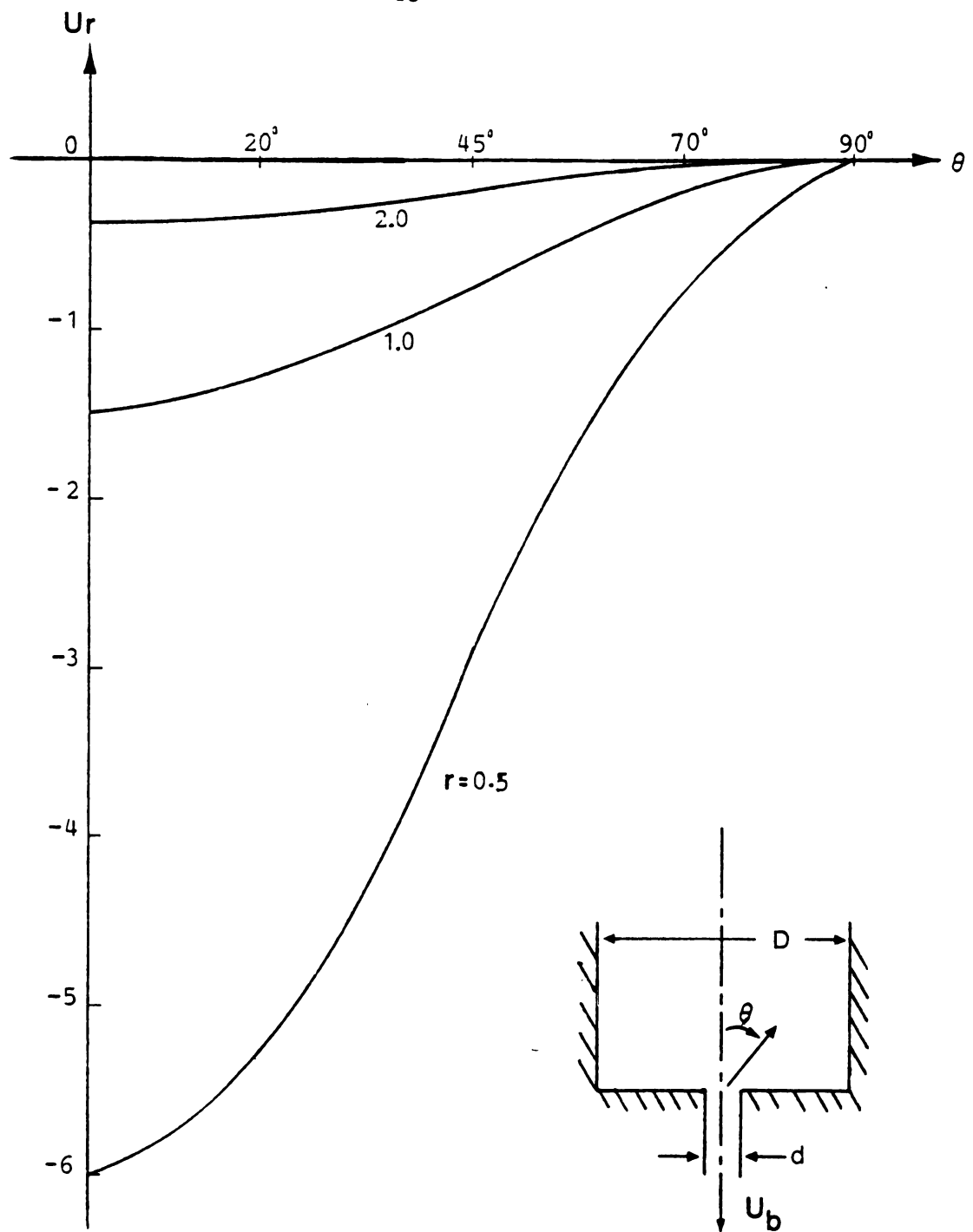The compressive and tensile stresses are given by

Figure 2.3. Velocity Distribution for Axisymmetric Conical Flow
of a Newtonian Fluid for d/D → 0
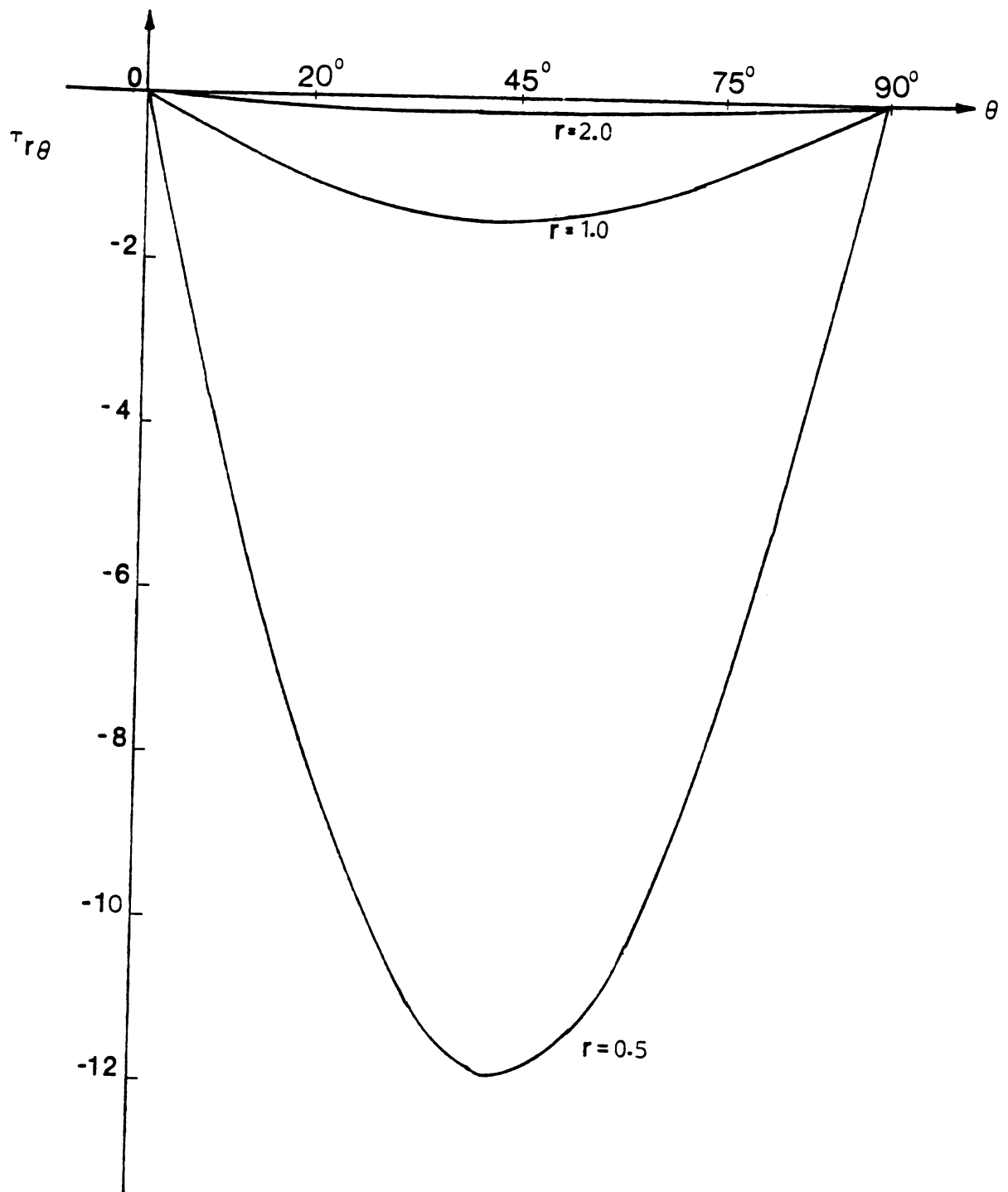
Figure 2.4.   Shear Stress Distribution for Axisymmetric Conical
Flow of a Newtonian Fluid for d/D → 0

$$\tau_{rr} = -6 \frac{\cos^2 \theta}{r^3} \tag{2.25}$$

$$\tau_{\phi\phi} = \tau_{\theta\theta} = 3 \frac{\cos^2 \theta}{r^3} \tag{2.26}$$

Note that

$$\tau_{rr} + \tau_{\theta\theta} + \tau_{\phi\phi} = 0 \tag{2.27}$$

Figure 2.5 shows that these normal stresses are an order of magnitude larger than the shear stresses for this flow. Thus, 'sink' flow should be an excellent kinematical model to develop insight regarding viscoelastic flows (Chapter 3).

The pressure distribution for W = 0 is given by

$$P = P_\infty + \frac{1 - 3\cos^2 \theta}{r^3} \tag{2.28}$$

Figure 2.6 shows that $P = P_\infty$ for $\theta = 54.75°$ and all $r > 0$. For $\theta < 54.75°$, $P < P_\infty$; and, for $\theta > 54.75°$, $P > P_\infty$. This qualitative feature of 'sink' flow has been verified experimentally by Bond [1925].

Figure 2.7 shows the locus of zero pressure for two different values of P_∞. Clearly no real flow will show this type of behavior and the 'bulge' where negative pressures occur will be replaced by another flow pattern having more than one velocity component. In
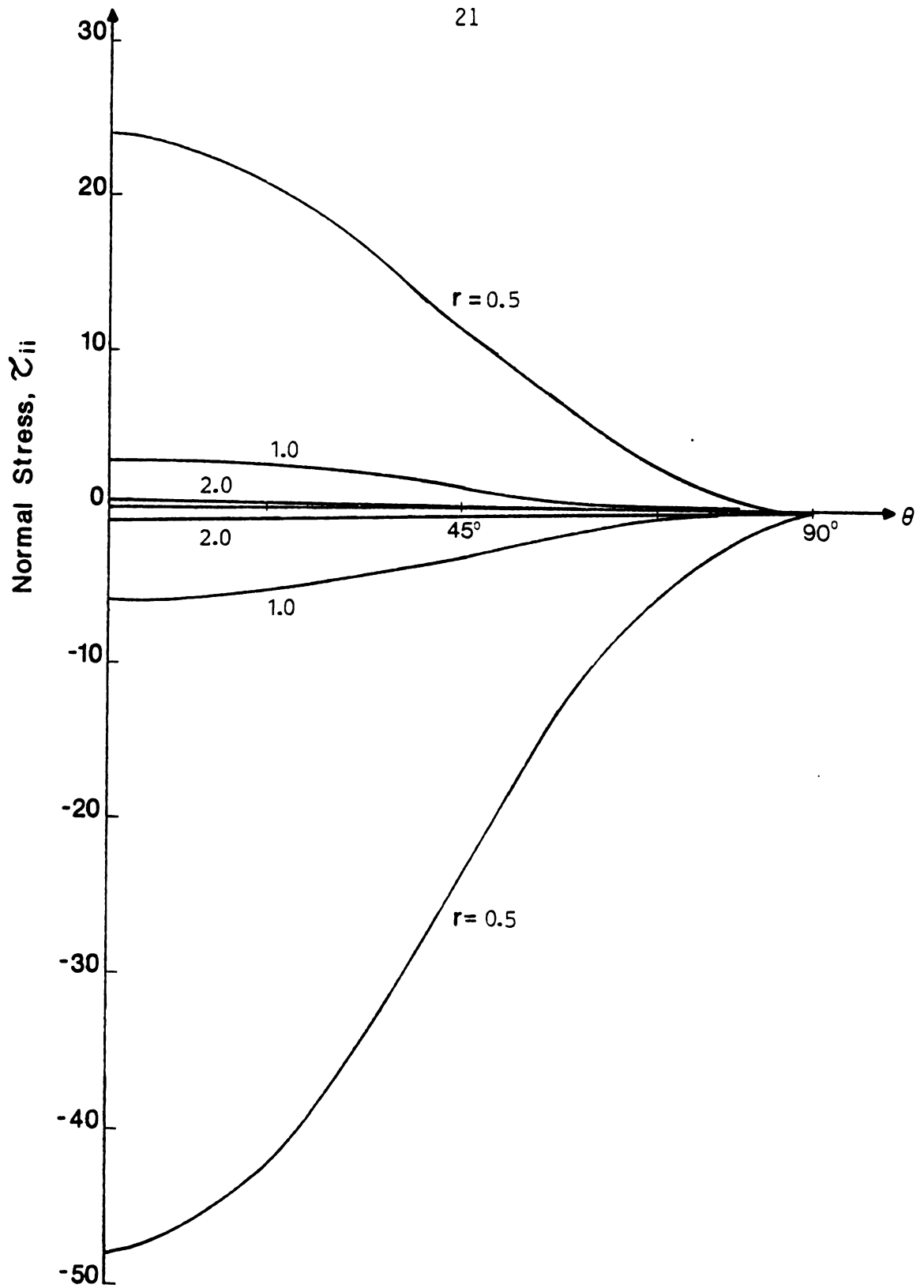
Figure 2.5   Distribution of Compressive and Tensile Stresses for
              Axisymmetric Conical Flow of a Newtonian Fluid for
              d/D → 0
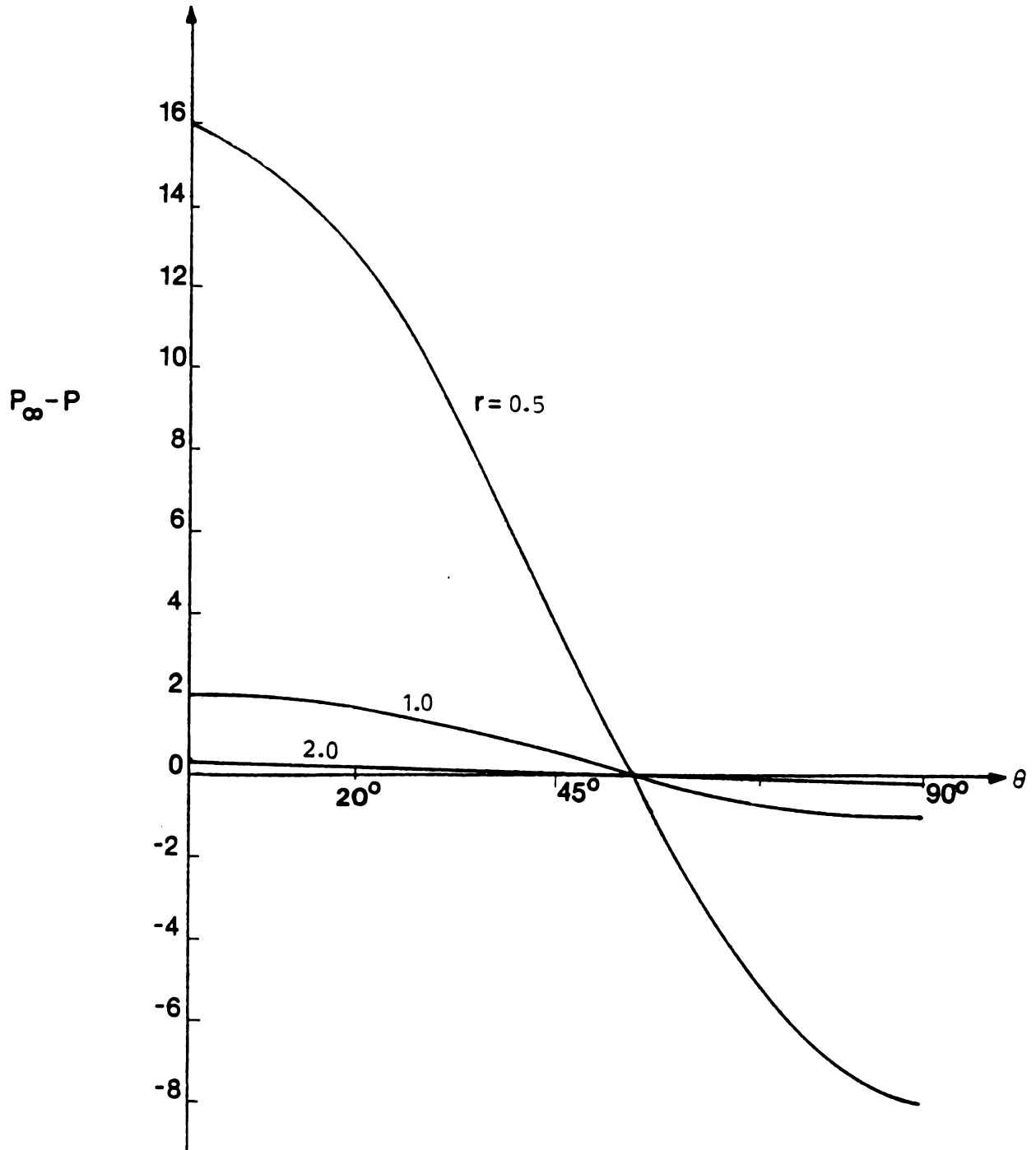
Figure 2.6   Pressure Distribution for Axisymmetric Conical Flow
of a Newtonian Fluid for d/D → 0

Figure 2.7   Locus of Zero Pressure for Axisymmetric Conical Flow
of a Newtonian Fluid for d/D → 0

the next chapter we examine the effect of elasticity on the distribution of stresses and, in particular, show how the negative bulge region changes with the Weissenberg number. An interesting result which follows is that for large enough W the region can be eliminated.

CHAPTER 3
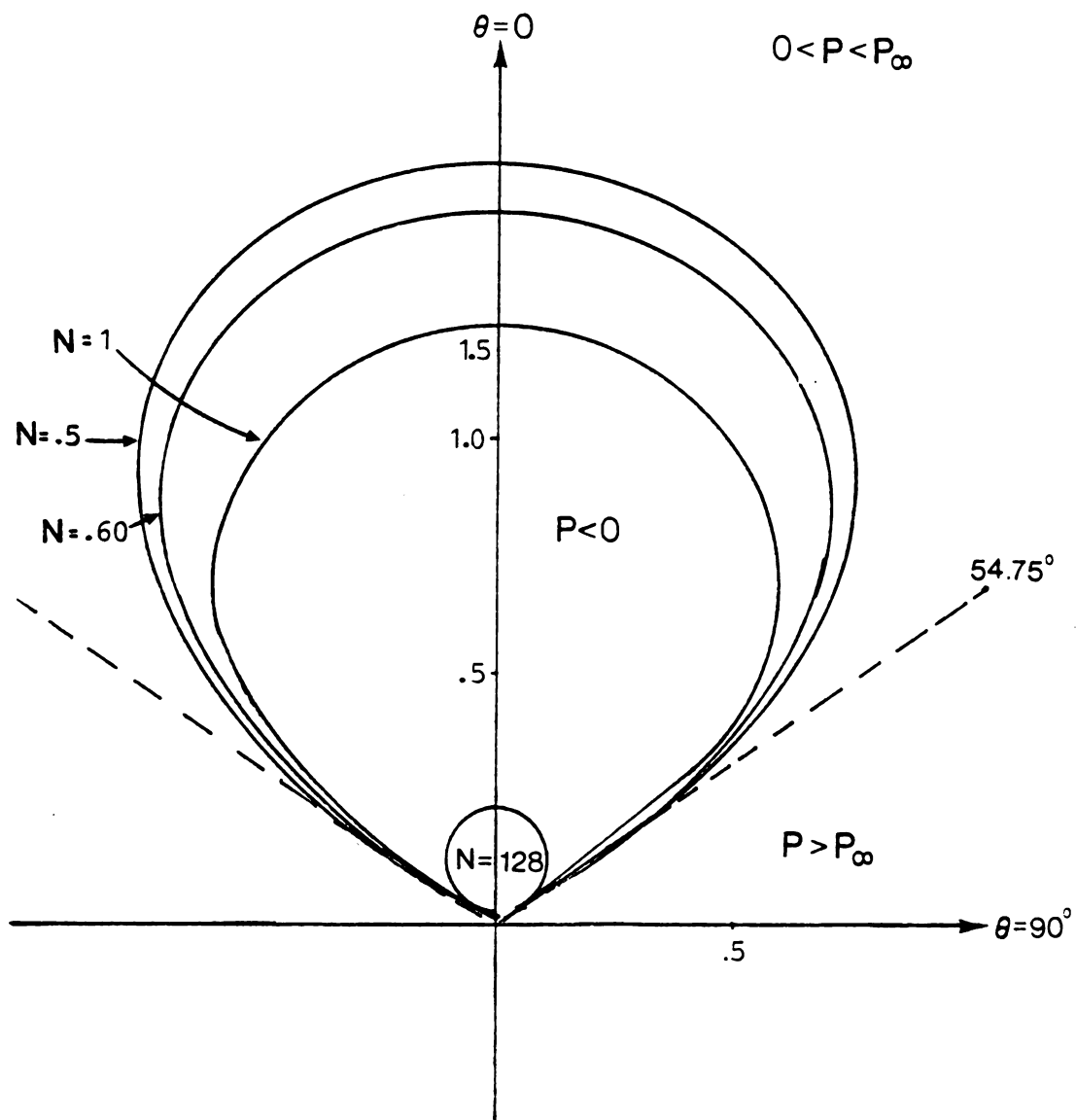
RESULTS AND DISCUSSION

Two approximations to the pressure field were examined. Both
approaches assume that the radial flow given by Equation (2.23)
can be used as a first approximation. Thus, the components of $\underline{\underline{\tau}}$
can easily be computed for this flow and from Equations (2.14)-(2.17)
we obtain

$$\tau_{rr} = \frac{3}{r^3}(1 + \cos 2\theta) + \frac{15}{4}\frac{W}{r^6}(1 + \cos 2\theta)^2 \tag{3.1}$$

$$\tau_{\theta\theta} = -\frac{3}{2r^3}(1 + \cos 2\theta) - \frac{9}{4}\frac{W}{r^6}(\cos 2\theta)(1 + \cos 2\theta) \tag{3.2}$$

$$\tau_{\phi\phi} = -\frac{3}{2r^3}(1 + \cos 2\theta) - \frac{9}{8}\frac{W}{r^6}(1 + \cos 2\theta)^2 \tag{3.3}$$

$$\tau_{r\theta} = \frac{3}{2r^3}(1 + \cos 2\theta) + 9\frac{W}{r^6}(1 + \cos 2\theta)\sin 2\theta \tag{3.4}$$

The isotropic pressure distribution to first order was calculated by simply integrating Equation (2.12). If u_r were an actual solution to Equations (2.12) and (2.13), then this would give the same result as integrating Equation (2.13). However, because W > 0, these two procedures yield different results because Equation (2.20) is not necessarily satisfied for u_r defined by Equation (2.23). Therefore, in what follows, Case A denotes the procedure which determines P so the radial component of the balance equation is satisfied everywhere. For Case B, Equation (2.13) is integrated from θ = 0 to θ. The pressure distribution for θ = 0 is determined by integrating (2.12) along the axis. Thus, this procedure yields a pressure field which satisfies the θ-component of the force balance everywhere and the radial component balance only on the axis. The two results are

Case A:

$$P_\infty - P = \frac{1}{r^3}\left(\frac{3\cos 2\theta + 1}{2}\right) - \tag{3.5}$$

$$\frac{W}{r^6}\left(8.25\cos 2\theta - 0.28\cos 4\theta + 8.53\right).$$

Case B:

$$P_\infty - P = \frac{1}{r^3}\left(\frac{3\cos 2\theta + 1}{2}\right) - \tag{3.6}$$

$$\frac{W}{r^6}\left(10.68\cos 2\theta - 4.5\cos 4\theta + 22.31\right).$$

The effect of the Weissenberg number on the pressure distribution for a fixed distance from the apex is illustrated in Figure 3.1a. Note the decrease in the critical angle where $P = P_\infty$ as W increases. Thus, as the elastic effect increases the amount of fluid driven to the contraction under a favorable pressure drop decreases. Furthermore, the magnitude of $|\Delta P|$ seems to be affected more on the axis ($\theta = 0$) than elsewhere. At $\theta = 90°$, W does not diminish $|\Delta P|$ at all.

Figure 3.1b shows that for W = 0.1 a fluid particle on the axis experiences more than a four-fold increase in ΔP over a distance of less than 2d. Thus, the fluid experiences a significant acceleration along this path. A comparable retarding effect (i.e., $\Delta P < 0$) occurs near the surface at $\theta = 90°$. Figure 3.1b seems to convey the idea that one mechanism near the axis causes the fluid to move toward the apex while another is responsible for flow toward the apex near the wall.

Figures 3.2a and b attempt to show most of the important qualitative effects of the Weissenberg number on the pressure distribution. First note the dramatic shift away from the Newtonian result (cf. Figure 2.7). For $P_\infty > 0.606$ and W = 0.1, a region of negative pressures no longer exists. Moreover, for fixed P_∞, increasing W also eliminates this phenomenon.

It is tempting to conjecture that the 'bulge' of negative pressures would be replaced in a real fluid by a secondary flow. Thus, a criteria for removing the existence of negative pressures
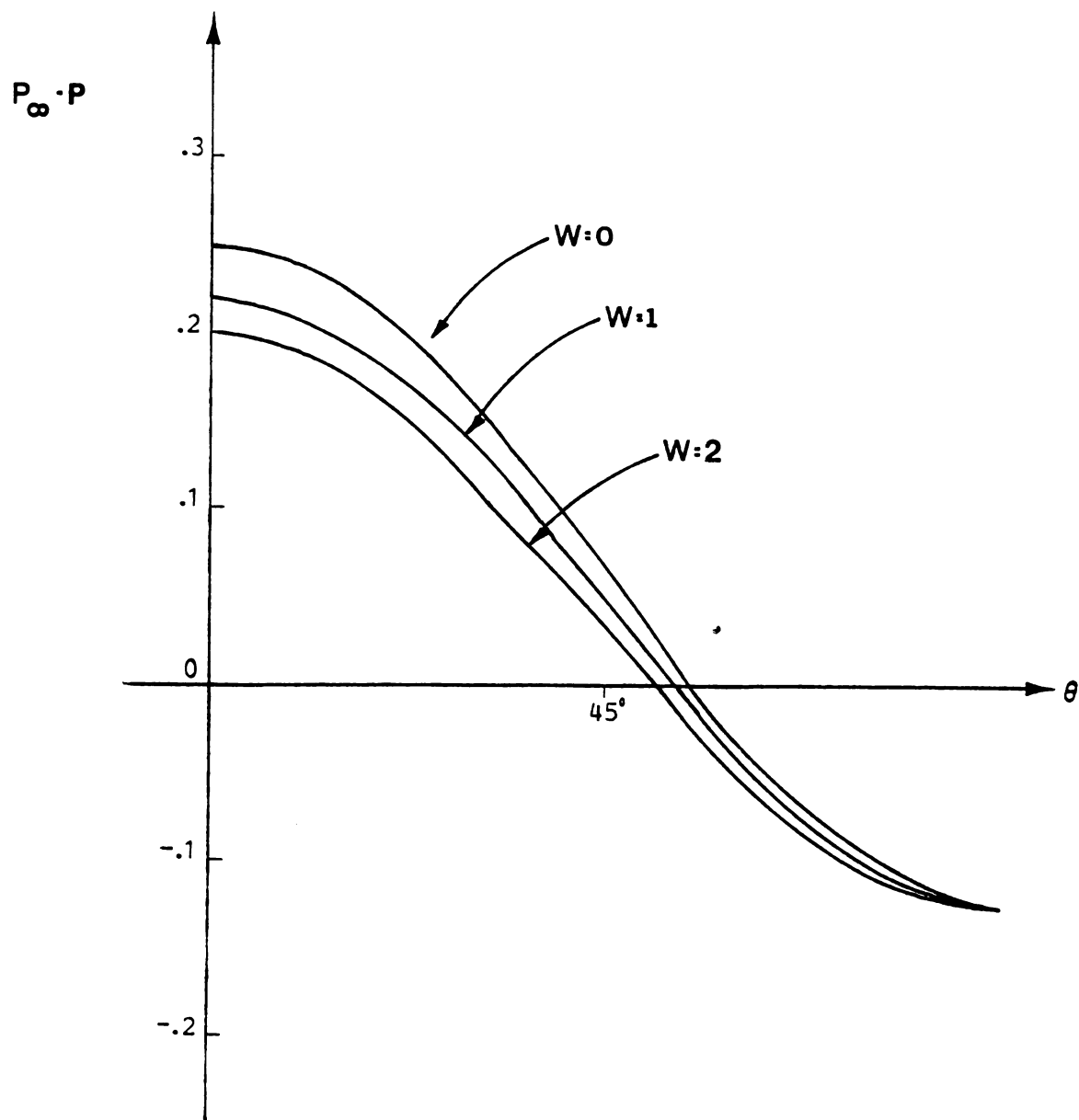
Figure 3.1a. Pressure Distribution for Axisymmetric Conical Flow of a Viscoelastic Fluid for d/D → 0 (constant r, Case A)

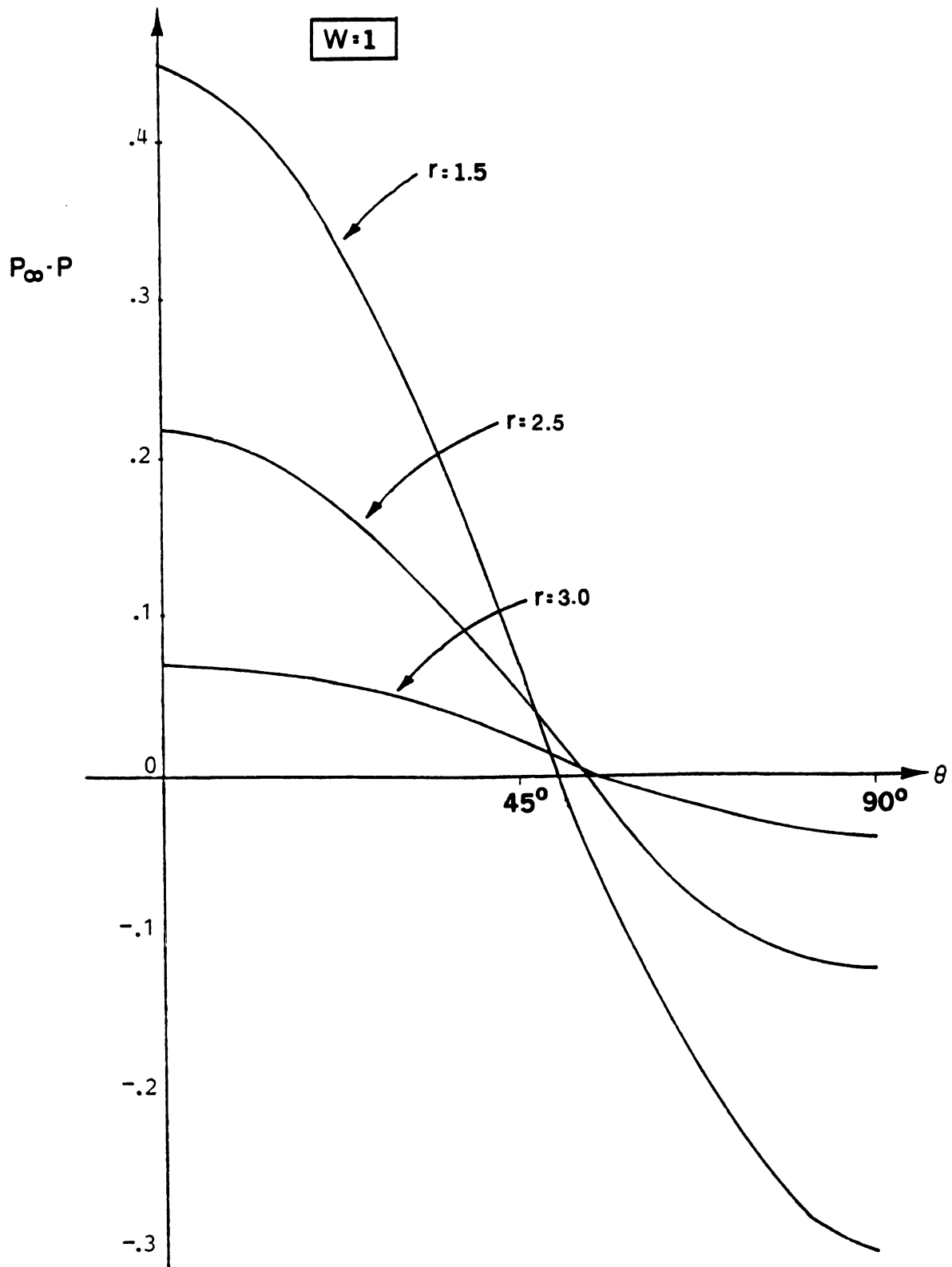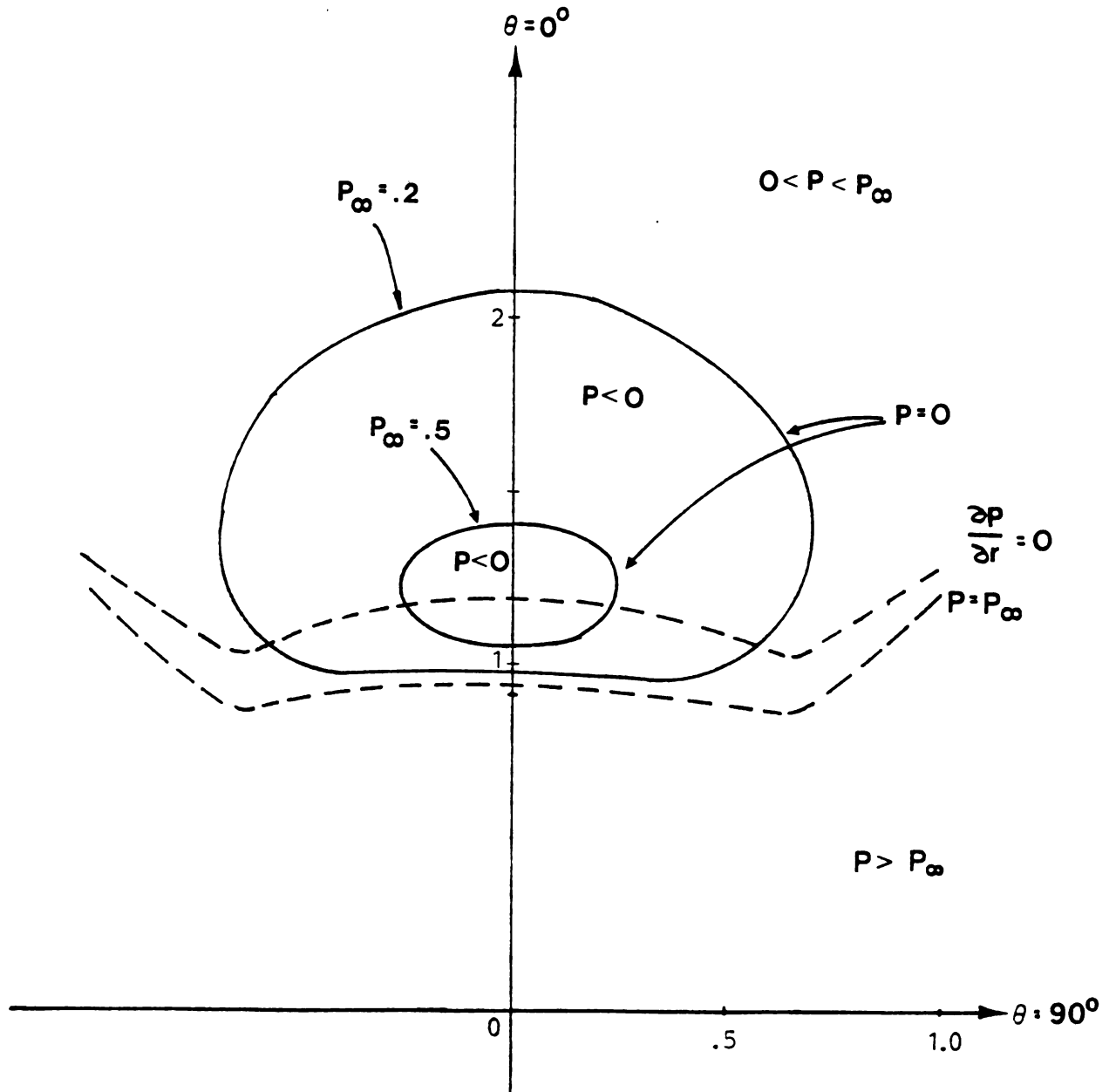Figure 3.1b. Pressure Distribution for Axisymmetric Conical Flow of a Viscoelastic Fluid for d/D → 0 (constant W, Case A)

Figure 3.2a. Locus of Zero Pressure for Axisymmetric Conical Flow
of a Viscoelastic Fluid for d/D → 0 (constant W,
Case A)
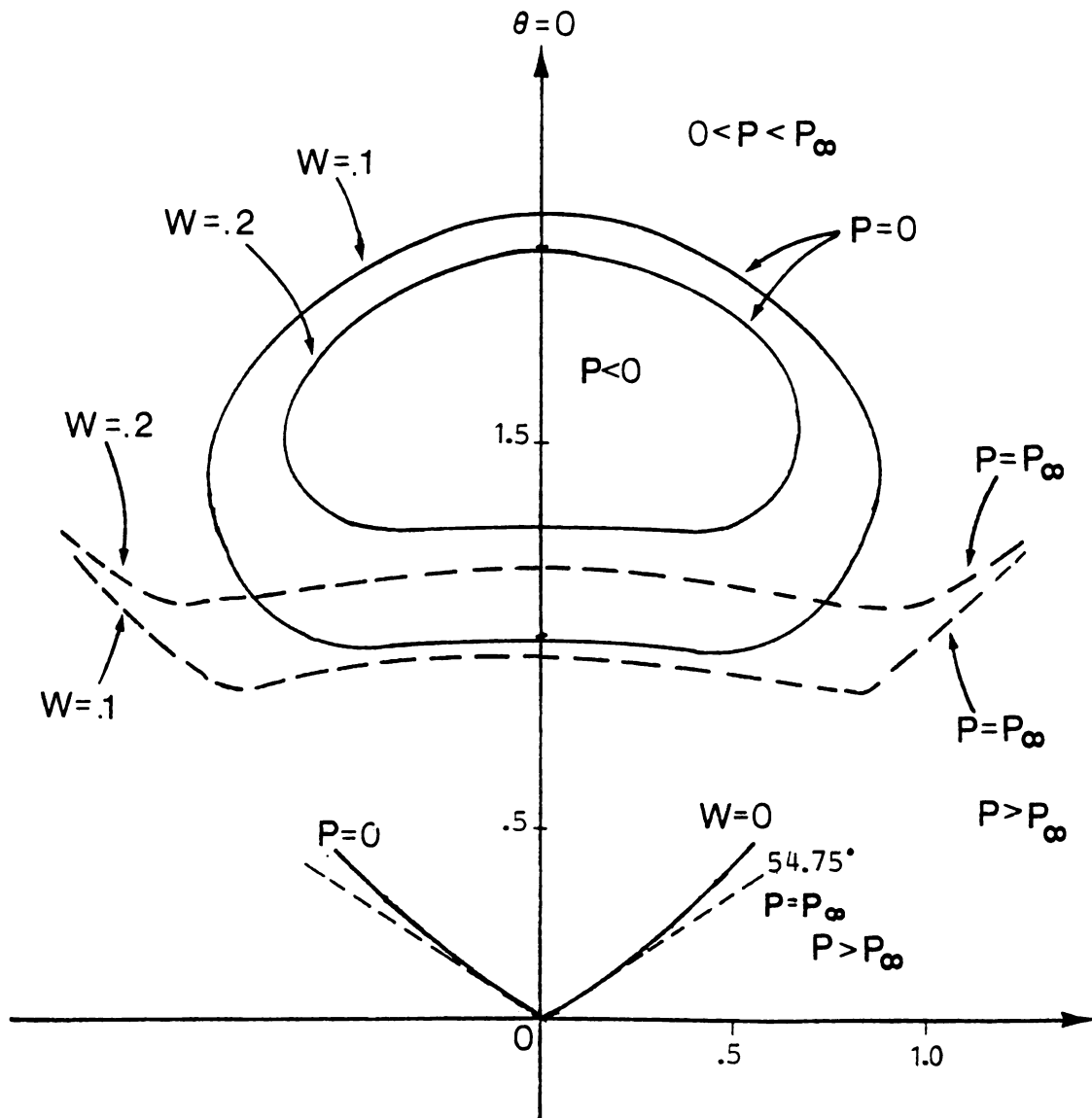
Figure 3.2b. Locus of Zero Pressure for Axisymmetric Conical Flow
of a Viscoelastic Fluid for d/D → 0 (constant P_∞,
Case A)

near the contraction becomes a stability criterion. Therefore,
we tentatively offer this observation as a hypothesis for further
study:

> *Instability Hypothesis.* A sufficient condition
> for the occurrence of a secondary motion on the axis
> of flow is

$$W P_\infty \; < \; 0.06 \tag{3.7}$$

Equation (3.7) follows directly from Equation (3.5) by setting $P = 0$
and determining the limits of the negative pressure 'bulge' on the
axis $\theta = 0$. If Inequality (3.7) is satisfied, then two real roots
exist.

Also shown in Figures 3.2a and b are lines of minimum pressure.
The physical significance of this is made clearer by examining
Figure 3.3. Note once again the dramatic effect the Weissenberg
number has on the isotropic pressure distribution. The result por-
trayed here shows that a positive minimum in P occurs about one
and a half diameters from the contraction. If the polymer were
saturated with air at $\hat{P}_\infty$, then 'hazing' would occur (see Figure 1.1c).
Figure 3.4 shows the variation of the total normal stresses on the
axis.

On the axis, r_o and r_m denote, respectively, the point where
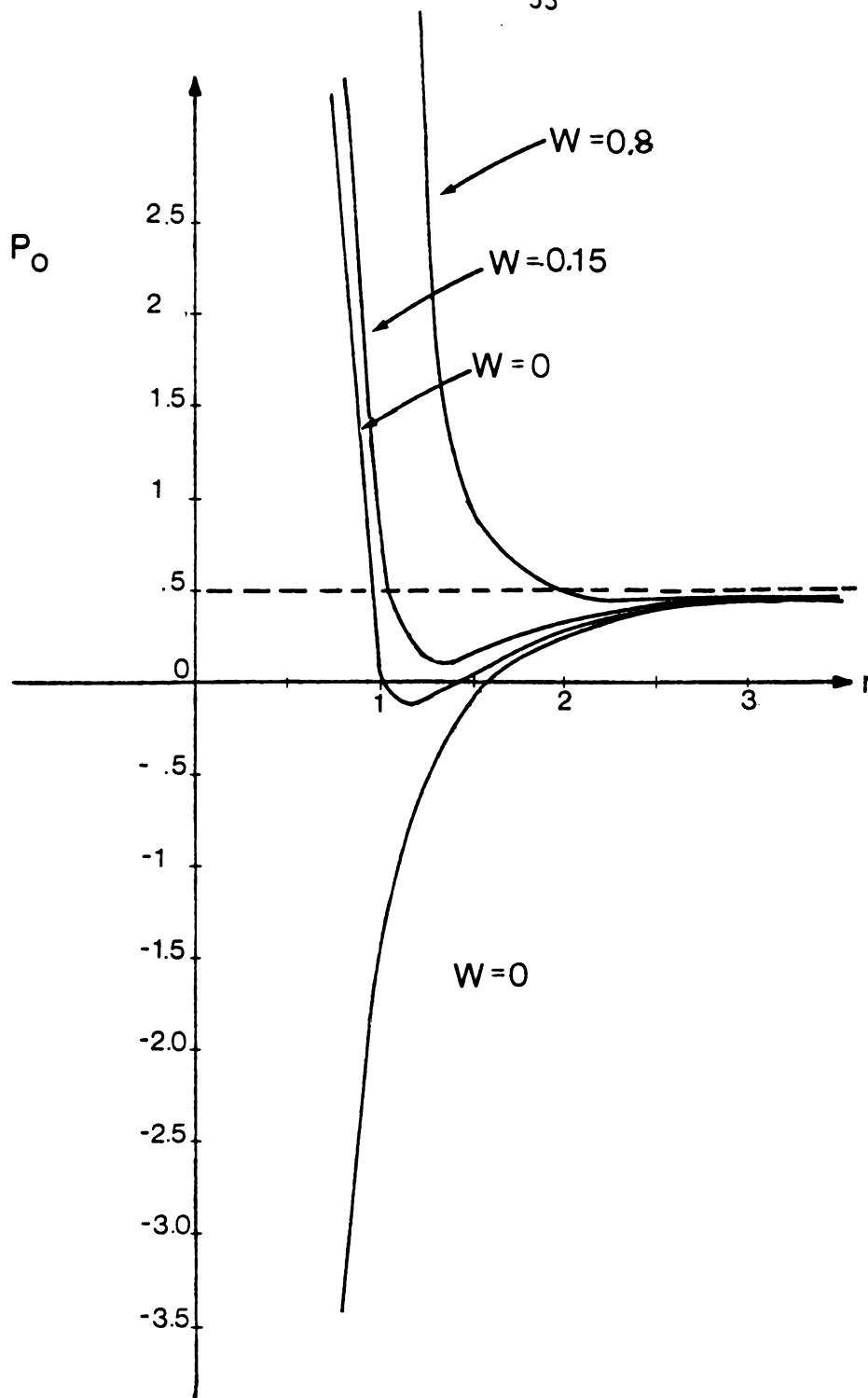$|\Delta P| = 0$ and the position of minimum pressure. From Equation (3.5)
it follows that

Figure 3.3. Pressure Distribution at Center Line for Axisymmetric
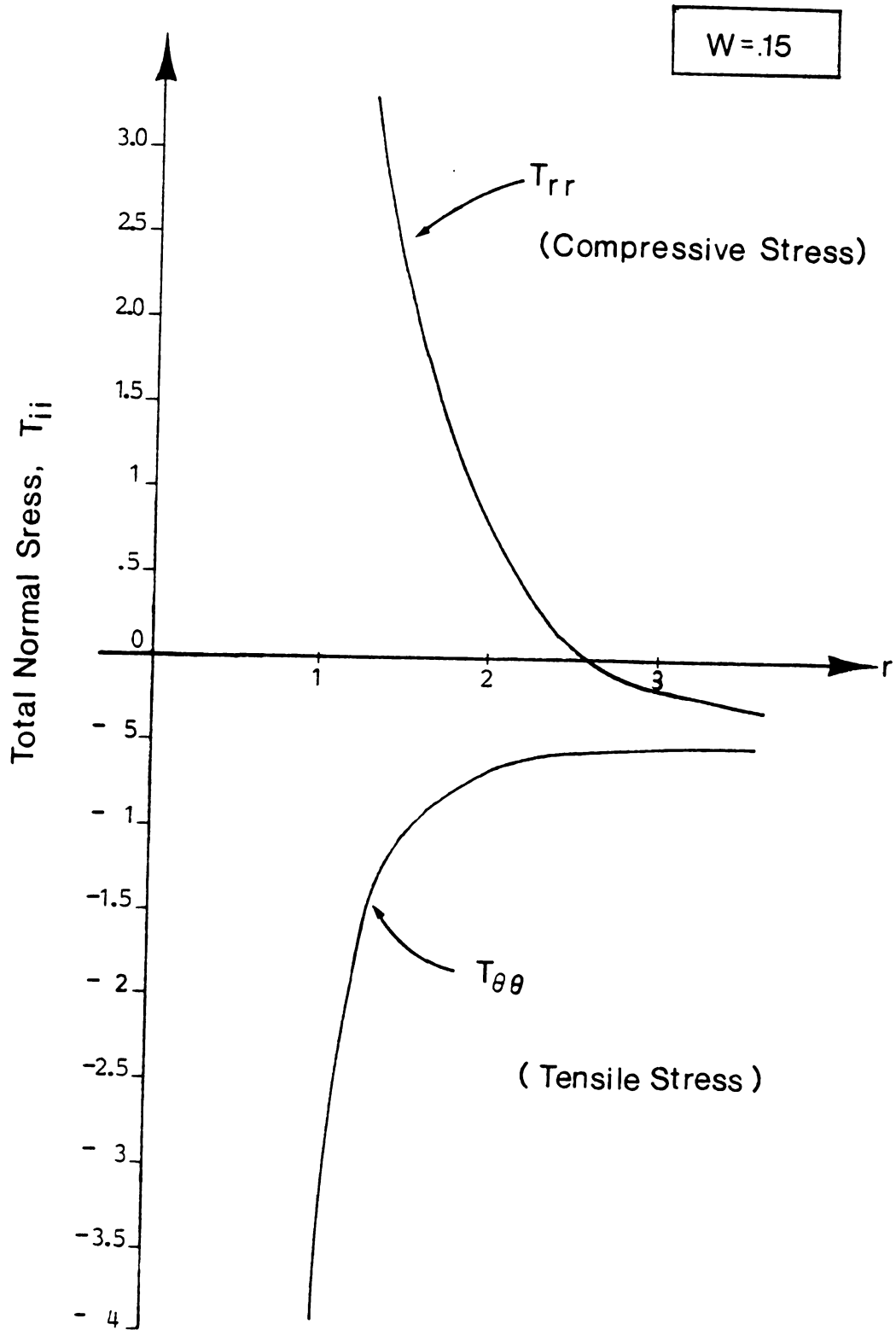Conical Flow of a Viscoelastic Fluid for d/D → 0
(Case A)

Figure 3.4. Distribution of Total Compressive and Tensile Stresses for Axisymmetric Conical Flow of a Viscoelastic Fluid for d/D → 0 (Case A)

$$r_o = 2.02 \ W^{1/3} \tag{3.8}$$

and

$$r_m = 2.54 \ W^{1/3} \tag{3.9}$$

The hazing phenomenon discussed by Metzner et al. [1969] could possibly be used to test these predictions.

Finally, Figure 3.5 shows how the size of the negative pressure 'bulge' varies with W for two values of P_∞. The parameter Δr_B simply denotes the width of this region on the axis. For a fixed Weissenberg number, say W = 0.25, the 'bulge' obviously does not exist for $P_\infty < 0.3$. However, by decreasing $\hat{P}_\infty$ or by increasing the flow rate Q (see Equation (2.4)) a 'bulge' will appear and may trigger an instability.

Figures 3.6a and b summarize the results obtained by calculating the pressure distribution using the θ-component of the force balance. Differences between this case and the previous one should be apparent.

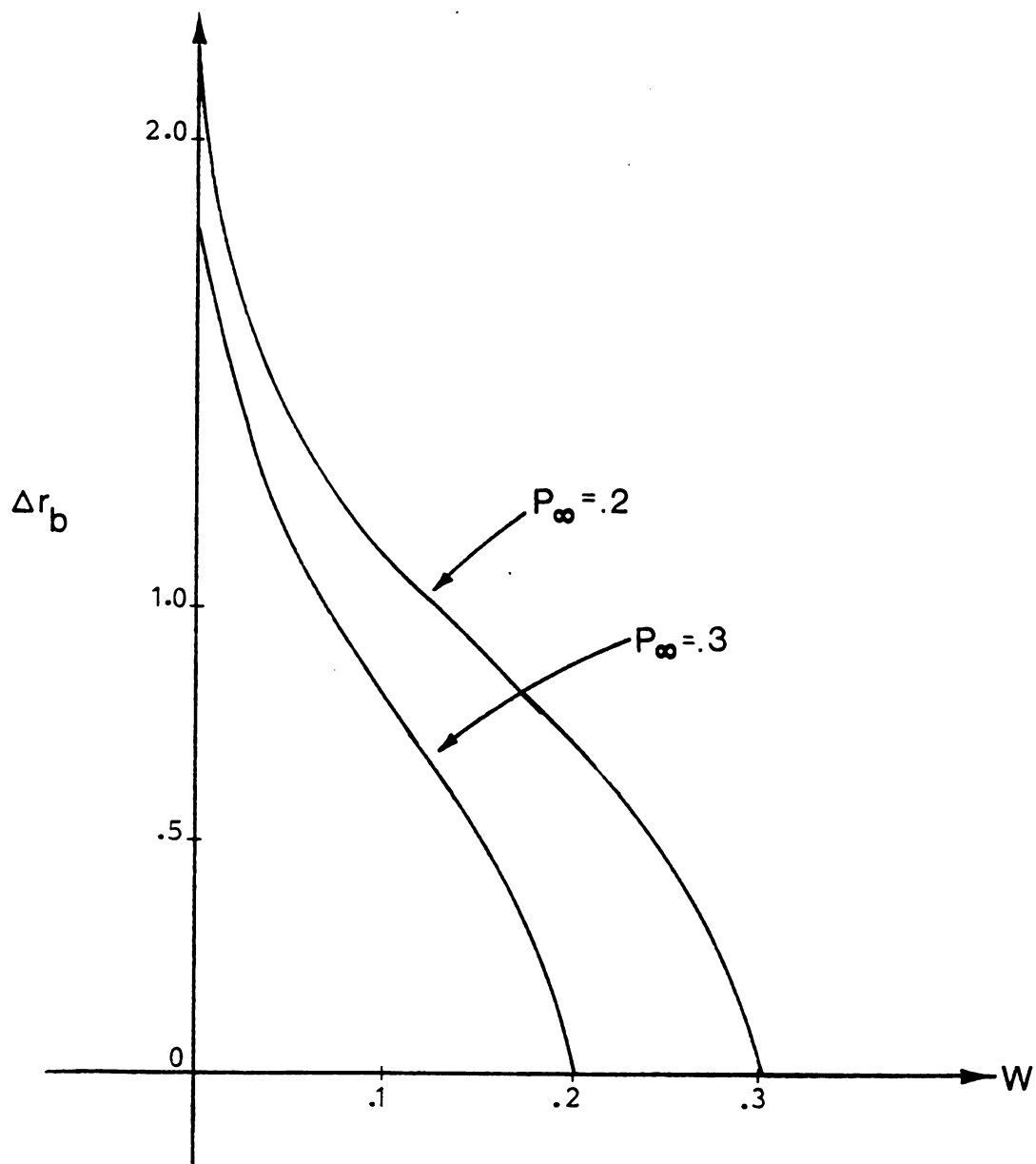Figure 3.5.   The Effect of Elasticity on the Growth of the 'Bulge'
Region for Axisymmetric Conical Flow of a Viscoelastic
Fluid for d/D → 0 (Case A)

Figure 3.6a. Locus of Zero Pressure for Axisymmetric Conical Flow
of a Viscoelastic Fluid for d/D → 0 (constant W,
Case B)
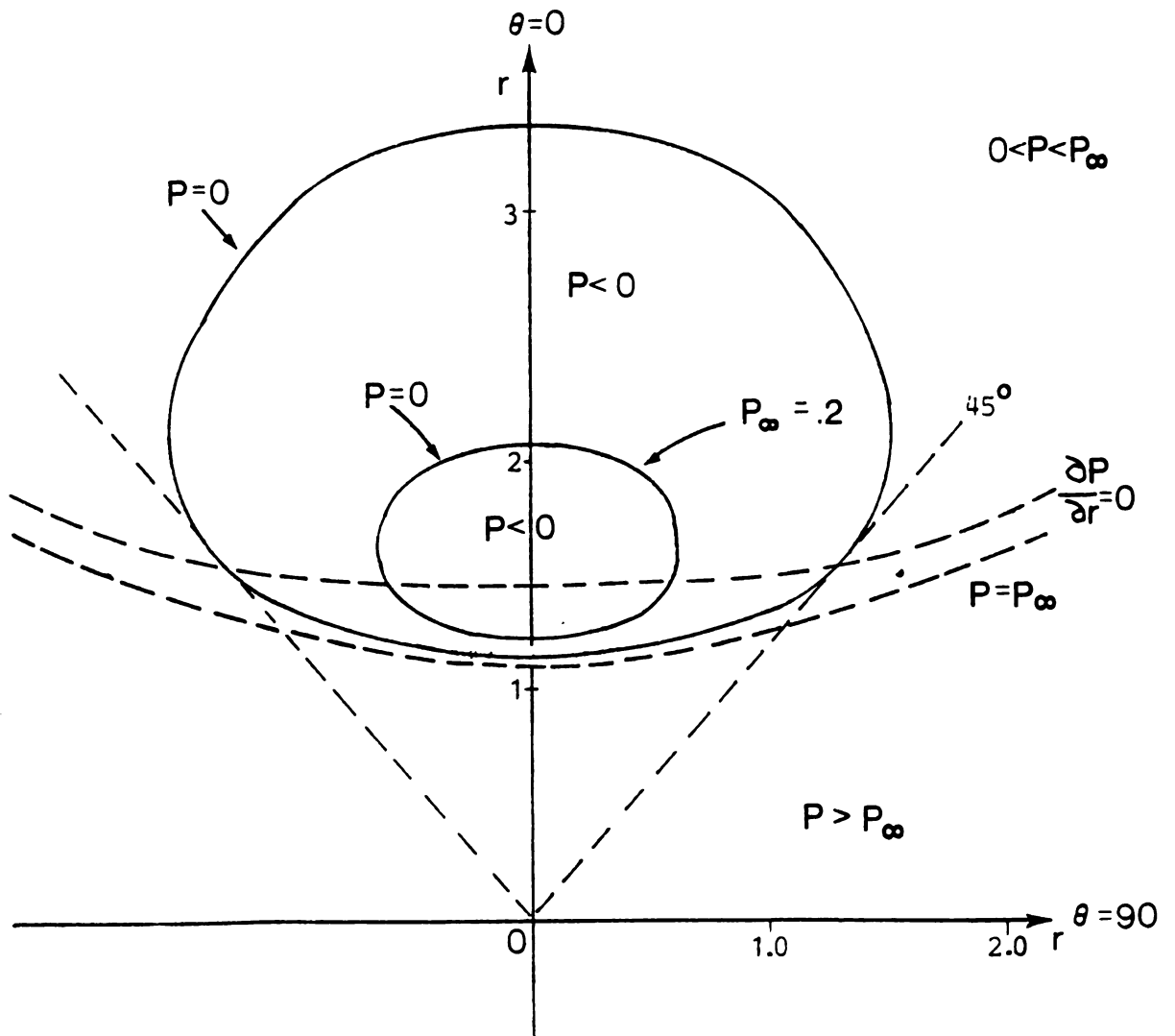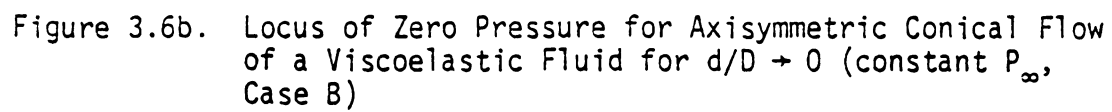
Figure 3.6b.   Locus of Zero Pressure for Axisymmetric Conical Flow
of a Viscoelastic Fluid for d/D → 0 (constant P∞,
Case B)

CHAPTER 4

CONCLUSIONS

First-order approximate pressure distributions for viscoelastic
fluids in conical flow were examined in this study. The results
show that under certain conditions a positive minimum in the isotropic
pressure occurs near the contraction. If the polymer were saturated
with air at $\hat{P}_\infty$, 'hazing' would occur at a location proportional
to one-third of the volumetric flow rate $(r_m \alpha Q^{1/3})$. A simple experi-
ment on the 'hazing' phenomenon is recommended to verify the predic-
tion. In addition, a negative pressure region was observed in this
study along the centerline near the apex. It was postulated that
this 'bulge' of negative pressure region would be replaced in a
real flow by second motions. A condition for removing these negative
pressures from the flow domain was derived. The result, which relates
the applied pressure $\hat{P}_\infty$ to the fluid viscosity and retardation time,
is

$$\frac{\lambda \hat{P}_\infty}{\mu} > 0.015$$

This interesting expression deserves further study.

LIST OF REFERENCES

LIST OF REFERENCES

Ackerberg, R.C., 1965. "The Viscous Incompressible Flow Inside a Cone," J. Fluid Mech. $\underline{21}$:1, 47.

Bhatnager, R.K., and Rajagopalan, R., 1967. "Secondary Flow of Rivlin-Ericken Fluids Between Two Concentric Spheres," Rheo Acta $\underline{6}$, 15.

Bird, R.B., Stewart, W.E., and Lightfoot, E.N., 1960. Transport Phenomena, Wiley, New York.

Black, J.R., and Denn, M.M., 1976. "Converging Flow of a Viscoelastic Liquid," J. of Non-Newtonian Fluid Mechanics $\underline{1}$, 83.

Bond, W.N., 1925. "Viscous Flow Through Wide-Angled Cones," Phil. Mag. $\underline{6}$, 1058.

Cable, P.J., and Boger, D.V., 1978a. "A Comprehensive Experimental Investigation of Tubular Entry Flow of Viscoelastic Fluids: Part I. Vortex Characteristics in Stable Flow," A.I.Ch.E.I. $\underline{24}$:5, 869.

_____, 1978b. "A Comprehensive Experimental Investigation of Tubular Entry Flow of Viscoelastic Fluids: Part II. The Velocity in Stable Flow," A.I.Ch.E.J. $\underline{24}$:6, 992.

Denn, M.M., 1980. Process Fluid Mechanics, Prentice-Hall, Englewood Cliffs, N.J.

Duda, J.L., and Vrentas, J.S., 1973. "Entrance Flow of Non-Newtonian Fluids," Trans. of the Society of Rheology $\underline{17}$:1, 89.

Harrison, W.T., 1920. "The Pressure in a Viscous Liquid Moving Through a Channel with Diverging Boundaries," Proc. Camb. Phil. Soc. $\underline{19}$, 307.

Kaloni, P.N., 1965a. "On Creeping Flow of a Viscoelastic Liquid in Converging Channel," J. of Phy. Society of Japan $\underline{20}$:1, 132.

_____, 1965b. "On the Flow of an Elastico-Viscous Fluid in a Conical Duct," J. of Phy. Society of Japan $\underline{20}$:4, 610.

Leslie, F.M., 1960. "The Slow Flow of a Viscoelastic Liquid Past a Sphere," Quant. J. Mech. and Applied Math. 14, 36.

Metzner, A.B., 1967. "Behavior of Suspended Matter in Rapidly Accelerating Viscoelastic Fluids: The Uebler Effect," A.I.Ch.E.J. 13:2, 316.

Metzner, A.B., Uebler, E.A., and Chan Man Fong, C.F., 1969. "Converging Flow of Viscoelastic Materials," A.I.Ch.E.J. 15, 750.

Oka, S., and Takami, A., 1967. "The Steady Slow Motion of a Non-Newtonian Liquid Through a Tapered Tube," Japanese J. of Applied Physics 6:4, 1967.

Perera, M.G.N., and Walters, K., 1976. "Long-Range Memory Effects in Flows Involving Abrupt Changes in Geometry," J. of Non-Newtonian Fluid Mechanics 2, 49.

Shümmer, P., 1967. "Zum Fließverhalten Nicht-Newtonscher Flüssigkeiten in Konischen Düsen," Rheo. Acta 6, 192.

Strauss, K., 1975. "Theoretical Rheology," Appl. Sci. Publ., Barking, p. 56.

Tanner, R.I., 1966. "Plane Creeping Flows of Incompressible Second-Order Fluids," The Physics of Fluids 9:6, 1246.

Uebler, R.B., 1966. "Pipe Entrance Flow of Elastic Liquids," Ph.D. Thesis, Univ. Delaware, Newark, Delaware.

Wagner, M.G., and Slattery, J.C., 1971. "Slow Flow of a Non-Newtonian Fluid Past a Droplet," A.I.Ch.E.J. 17:5, 1198.